Hue University Journal of Science: Natural Science
Vol. 133, No. 1B, 109–123, 2024

pISSN 1859-1388
eISSN 2615-9678

Study on the antifungal potential of *Piper betle* methanol extract against *Colletotrichum gloeosporioides* cutinase

Nguyen Thi Ai Nhung[1]*, Nguyen Thi Thanh Hai[1], Thanh Q. Bui[1], Nguyen Vinh Phu[2], Phan Tu Quy[3]

[1] Department of Chemistry, University of Sciences, Hue University, Hue, Vietnam
[2] Faculty of Basic Sciences, University of Medicine and Pharmacy, Hue University, Hue, Vietnam
[3] Department of Natural Sciences & Technology, Tay Nguyen University, Buon Ma Thuot, Vietnam

* Correspondence to Nguyen Thi Ai Nhung <ntanhung@hueuni.edu.vn>
(*Received: 13 March 2024; Revised: 03 April 2024; Accepted:09 April 2024*)

Abstract. *Piper betle* methanol extract and its compositional characteristics had been evidenced for their effective inhibitability against rice-blast fungus. In this work, they were subjected for further computational efforts to complete their bio-chemo-pharmacological profile, and broaden their anti-fungal potentiality against *Colletotrichum gloeosporioides* cutinase presentative (PDB-3DEA). As the results, the most noticeable promising inhibitors particularly regard to **5** (DS -10.8 kcal.mol^{-1}; ground-state energy -499.50 a.u.; dipole moment 2.61 Debye; no toxicity; content 49.90 %) and **6** (DS -10.9 kcal.mol^{-1}; ground-state energy -652.15 a.u.; dipole moment 2.82 Debye; no toxicity; content 13.23 %), given by both their natural contents and predicted properties. The theoretical retrievals would reinforce the antifungal activities of *P. betle* and be conducive to further efforts to develop a green fungicidal alternative with broad-spectrum and cost-effective pesticidal advantages.

Keywords: *Piper betle* L, *Colletotrichum gloeosporioide*, *in silico*, ethanol extract, fungicidal alternative

1 Introduction

Recently, due to the overuse of antibiotics in the treatment of infectious diseases, multi drug resistance in human, animal and plant pathogens is very common. Therefore, there is an urgent need to find new antimicrobial compounds from various sources. Natural products have become increasingly interested; e.g. medicinal plants and their derivatives may provide alternative antimicrobial compounds [1,2].

The hot pepper plant (*Capsium frutescens* L) is a member of the Solanaceae family and widely grown in tropical and subtropical countries [3]. Hot peppers are sodium-low, cholesterol-free, rich in vitamins A and C; the plants are also known as a good source of potassium, folic acid, and vitamin E. Particularly, fresh green hot peppers have higher contents of vitamin C than that of citrus fruits; while, fresh red hot peppers have more vitamin A than carrots [4]. Regarded as household cooking spices, hot peppers are often consumed as fresh fruit, young leaves, or processed as salt sour, sauces, juices, and dried powders. In terms of health benefits, hot peppers are respected as a valuable source for treatment of various diseases given by the folk medication [5]. In Vietnam, hot pepper is one of the important agricultural products, contributing largely to the gross export value. Worldwide, although hot pepper is an important spice crop, the plant is often known for being vulnerable to many microbial diseases, leading to yield reduction and crop loss in general.

Among causes affecting hot pepper reduced cultivation, anthracnose disease has been often recognized as the most detrimental one, whose

origin is of the infection of *Colletotrichum* species. This disease is characterized by very dark, sunken lesions, containing spores [6], directly reducing the quality and quantity of the harvest. *Colletotrichum* is a large genus of Ascomycete fungi, containing species that cause anthracnose diseases on many economically important crops [7], including hot pepper [8]. In particular, *Colletotrichum gloeosporioides* has been reported as the most commonly seen causative agent relating to anthracnose disease and postharvest decay on a wide range of tropical, subtropical, and temperate fruits, crops and ornamental plants [9,10]. A variety of surveys in different countries revealed that the yield losses by anthracnose can be upto 80 %, e.g.: India (10-54 %), Korea (10 %), Vietnam (20-80 %) [11–13].

Therefore, if viral proteins of the fungus are inhibited to a certain degree, fungal infection can be of deterrence. A promising target is cutinase, a group of enzymes that are found to be secreted by both fungi and bacteria. These enzymes induce the cleavage of the ester bonds of cutin in the extracellular structures of the host plants, resulting in degradation of cell walls [14]. This means that an effective inhibition against these enzymes might help prohibit the spread of fungus onto the hot peppers in general. The crystal structure of *C. gloeosporioides* cutinase was already determined and deposited on RCSB Protein Data Bank (RCSB PDB) for public reference under the entry: 3DEA (DOI: 10.2210/pdb3DEA/pdb).

Regarding pesticidal management methods, the use of chemicals is a widely used disease control strategy and a practical method for the control of anthracnose disease. Typically, azoxystrobin is a broad-spectrum systemic fungicide widely used in agriculture to protect crops from fungal diseases. The fungicide was first-time introduced to the market under the brand name Amistar in 1996. After that, it had gained registration in 48 countries and was officially approved for use on over 50 different crops by 1999. Most recently, it was granted the prestigious UK Millennium product status in the year 2000 [15]. However, fungicidal resistance often arises quickly if a single compound is relied upon too heavily [16]. Furthermore, there are many undesirable effects of using chemicals such as prolonging persistence, human-health toxicity, and environmental pollution [17]. Fortunately, Betel vine (*Piper betle* L.), belonging to the genus Piper of the family *Piperaceae*, is considered as a promising alternative source for agricultural protectants. It is a popular medicinal plant mainly found in east Africa and the tropical regions of Asia [18]. In these countries, there are many products made from *P. betle* such as toothpaste, shampoo, personal care products, herbal supplements and herbal drinks [19–22].

Recent researches have shown solid evidences on the anti-microbial activities of *P. betle* products. The leaf-based extracts exhibited the antibacterial activity against a variety of gram-negative and gram-positive bacteria, including *Escherichia coli*, *Pseudomonas aeruginosa*, *Staphylococcus aureus*, *Candida albicans* [23,24]. Besides, the crude of *P. betle* leaf extracts could be effective against various fungal species including *Aspergillus flavus, Aspergillus fumigatus, Aspergillus niger, Aspergillus parasiticus, C. albicans, Candida glabrata, Candida krusei, Candida neoformans, Candida parapsilosis, Candida tropicalis, Epidermophyton floccosum, Trichophyton mentagrophytes, Trichophyton rubrum, Microsporum canis, and Microsporum gypseum* [24].

In our previous work, *P. betle* methanol extracts were proven for their effective inhibitability, both experimentally and computationally [25]. Regarding lab-based attempts, the extracts were obtained by maceration method; the compositional components were

pISSN 1859-1388
eISSN 2615-9678

characterized by gas chromatography - mass spectrometry (GC-MS); the bio-activities against the fungus were proven against rice-blast fungus *Magnaporthe oryae*. Regarding computer-based analyses, the candidate structures were subjected to molecular docking simulation (against *M. oryae* trehalose-6-phosphate synthase structure) and physicochemical predictions (by QSARIS).

In this extension, the *P. betle* methanol-extract data was subjected again for further computational efforts to complete their bio-chemo-pharmacological suitability in particular, and broaden their anti-fungal potentiality in general. The investigating candidates were those already identified from the experimental characterization; the corresponding components were analyzed by density functional theory (DFT) calculation (for chemical appropriateness), molecular docking simulation (against *C. gloeosporioides* cutinase structure), and statistical regressions (for pharmacological suitability).

2 Methodology

2.1 Literature review

The presence of active compounds and their percentage in ethanol extract from *Piper betle* leaves were already determined by GC-MS analysis in our previous report, including 14 phytochemicals [25]. The data was re-collected to be serving as the precursor input for the extensive computational efforts in this work.

2.2. Quantum chemical calculation

Molecular quantum properties were obtained from density functional theory (DFT) calculation on Gaussian 09: no symmetry constraints [26]; level of theory M052X/6-311++g(d,p) [27,28]. The global minimum on the potential energy surface (PES) was confirmed by vibrational frequencies. The frozen-core approximation for non-valence-shell electrons and the resolution-of-identity (RI) approximation were applied. The criterion of convergence for the SCF energy was set to 10^{-8} a.u.; and the modified integration grid "m4" was used. The configurations were used for the calculation of optimized geometries, potential energy surface (PES), and dipole moments at the same level of theory M052X/6-311++g(d,p). NBO 5.1 was utilized to converge the frontier orbital analysis at the level of theory M052X/def2-TZVPP for the molecular electrostatic potential (MEP) in the molecule which was calculated and visualized by GaussView 05 software.

2.3. Molecular docking simulation

Ligand-protein static inhibitability can be evaluated using MOE 2022.10 [29] based on the molecular docking technique. In a typical procedure, the simulation follows four steps and results in ligand-protein complex structures, accordingly.

(i) Input preparation: Protein 3DEA were referenced from public online protein banks; active-gird range: 4.5 Å from amino acids; force field: MMFF94x; Tether-Receptor strength: 5000; energy resolution: 0.0001 $kcal.mol^{-1}.Å^{-1}$. Ligand structures were from those selected from our previous works; geometrical optimization: Conj Grad algorithm; energy-change termination: 0.0001 $kcal.mol^{-1}$; charge assignment: Gasteiger-Huckel method.

(ii) Docking simulation: Ligand-protein interaction was simulated; number of retaining poses = 10; maximum solutions per iteration = 1000; maximum solutions per fragmentation = 200.

(iii) Re-docking iteration: The inhibitory components (ligand and protein) were separated, then re-docked. The accuracy of the docking protocol is justified if RMSD values (of docked and re-docked conformations) are all under 2 Å.

(iv) Theoretical interpretation: The primary parameters for inhibitory effectiveness are docking score (DS) energy, root-mean-square deviation (RMSD) value, and numbers of hydrophilic binding (hydrogen-like bonds). Besides, ligand-protein interactions and in-pose arrangement were mapped and rendered on 2D and 3D visualization, respectively.

2.4. ADMET analysis

ADMET properties (absorption, distribution, metabolism, excretion, and toxicity) were obtained from a web-based regressive model developed and maintained by the Molecular Modeling Group, Swiss Institute of Bioinformatics, i.e. SwissADME (http://www.swissadme.ch/; March 12th, 2024). The theoretical interpretations of output pharmacokinetic parameters were described by Pires et al. [30].

Table 1. Identification of bioactive compounds in *Piper betle* L. [25]

Notation	Subtance	Formula	Percentage (%)
1	Chavicol	$C_9H_{10}O$	0.48
2	Eugenol	$C_{10}H_{12}O_2$	7.88
3	β-Caryophyllene	$C_{15}H_{24}$	1.22
4	α-Caryophyllene	$C_{15}H_{24}$	0.19
5	4-Chromanol	$C_9H_{10}O_2$	49.90
6	1′-Hydroxychavicol acetate	$C_{11}H_{12}O_3$	13.23
7	Eugenol actate	$C_{12}H_{14}O_3$	3.45
8	4-Allyl-1,2-diacetoxybenzene	$C_{13}H_{14}O_4$	11.77
9	Phytol	$C_{20}H_{40}O$	0.33
10	Phytol actate	$C_{22}H_{42}O_2$	0.94
11	Vitamin E	$C_{29}H_{50}O_2$	0.51
12	Campesterol	$C_{28}H_{48}O$	0.51
13	Stigmasterol	$C_{29}H_{48}O$	0.55
14	Beta-Sitosterol	$C_{29}H_{50}O$	2.49

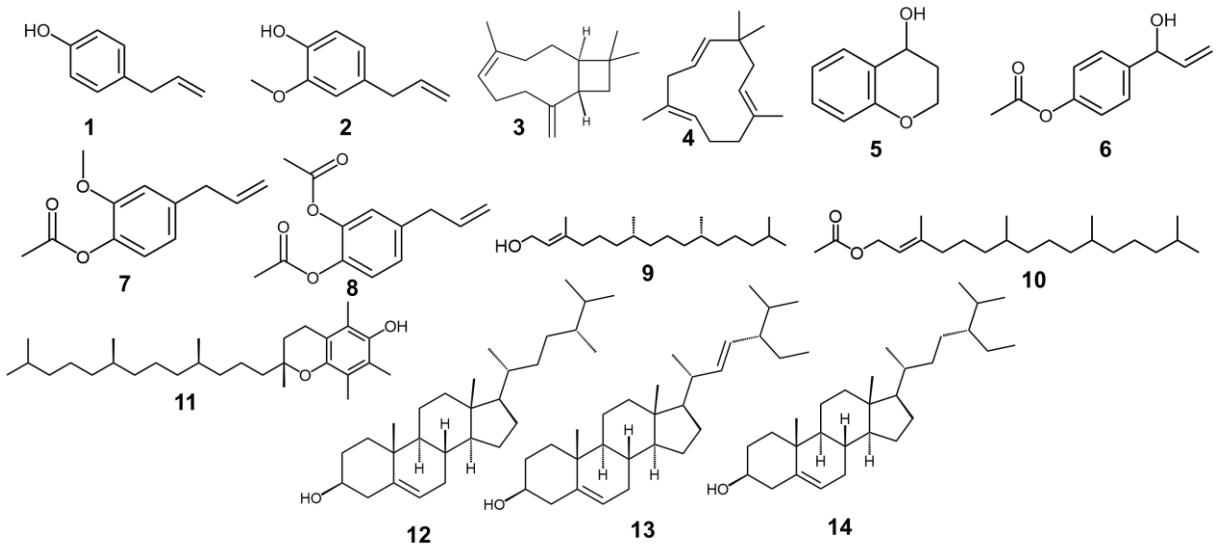

Fig. 1. Chemical structure of isolated compounds in *Piper betle* L. ethanol extract

pISSN 1859-1388
eISSN 2615-9678

3 Results and discussion

3.1 Chemical composition

The presence of active compounds and their percentage in ethanol extract from *P. betle* leaves were already determined by GC-MS analysis in our previous report, including 14 phytochemicals. The most predominant constituent is 4-Chromanol (**5**; 49.90 %), accounting for half of the total extract; it is followed by the other major parts, i.e.: 1'-Hydroxychavicol acetate (**6**; 13.23 %), 4-Allyl-1,2-diacetoxybenzene (**8**; 11.77 %), and Eugenol (**2**; 7.88 %). They together make up the proportion of over 80 %. For convenience, the data is recited into Table 1 and the corresponding structural formulae were presented in Figure 1; herein, they are used as the input for the computational models in this work.

3.2 Quantum-based chemical properties

The output of quantum calculations includes optimized structural geometry and electronic configurations, thereby providing valuable *ab initio* insights into chemical activities within intermolecular interactions. These insights are given by the intrinsic chemical properties of each bioactive compound (**1-14**), independent of any specific reference to targeted proteins.

Figure 2 illustrates the converged geometries of the studied compounds. Overall, convergence is achievable without imposing geometrical constraints or encountering abnormal bonding parameters (such as angles and lengths). This indicates stability akin to natural compounds, thereby corroborating our previous spectroscopic characterization and structural elucidation. Notably, the bond lengths exhibit marginal variations within characteristic ranges: C-C (appx. 1.5 Å), C=C (appx.1.3 Å), C-H (appx.1.1 Å), C-O (appx.1.4 Å), C=O (appx.1.2 Å); furthermore, the aromatic ring maintains planarity.

Their molecular properties of interest are summarized in Table 2, including ground state energy and dipole moment. The former represents chemical inactivity while the latter defines the positive-negative charge separation in a system. Their negative ground-state energy signifies electronic stability, implicating them less susceptible to chemical reactions and more conducive to non-chemical interactions. This, on the other hand, is thought to be conducive to ligand-protein inhibition; especially, **10-11** (below -1000 a.u.) register the values of most significance. Given dipole moment values, **2**, **5-7**, **9-10**, and **13** (over 2 Debye) possess predominant values; meanwhile, the corresponding figure for **3** (0.39 Debye) and **4** (0.46 Debye) are most marginal. In summary, the primary constituents of *P. betle* extract also belong to the group of highest suitability for biological applications in general and protein-inhibited interactions [31].

Figure 3 presents the highest occupied molecular orbital (HOMO) and lowest unoccupied molecular orbital (LUMO) of the optimized structures. Particularly, **1-8** had the localization of electron densities distributed evenly and largely over their molecular plane regarding both HOMOs and LUMOs. According to the theoretical charge-transferring properties, HOMO represents an intermolecular electron donation tendency, and LUMO represents an electron-accepting ability. In theory, this means that the host molecules are highly flexible for intermolecular interaction. Besides, negligible electronic densities were given by either HOMO or LUMO, implicating almost inert chemical activation. Quantitatively, all structures are considered to exhibit electronic stability of very high significance given low E_{HOMO}, all under -7 eV (while commonly agreed under -5 eV); in addition, their insulation–semiconduction band-gap energy ($3.2\ eV < \Delta E_{GAP} < 9\ eV$) [32] might suggest intermolecular binding capability toward polypeptide structures, whose electric conductivity was well-observed and explained based on superexchange theory (or electron tunneling) [33,34].

Figure 4 presents molecular electronic potential (MEP) maps of the optimized structures, indicating the distribution of chemical activities across their molecular plane. Conventionally, reddish colors signify regions with a negative electrostatic potential, indicating a high electron density. These areas typically act as nucleophilic sites in chemical reactions while functioning as electron donors in intermolecular interactions. Conversely, bluish colors denote positive electrostatic potential, associated with electrophilic reactivity. Whitish colors, on the other hand, represent neutral regions, exhibiting tendencies unlikely to align strongly with either nucleophilic or electrophilic behavior. Overall, all the compounds appear to localize their chemical tendencies around their main functionals rather than over their molecular planes. From a theoretical argument, this means they are less likely to have flexibility to form hydrophilic bonds, yet more likely to rely on hydrophobic interactions.

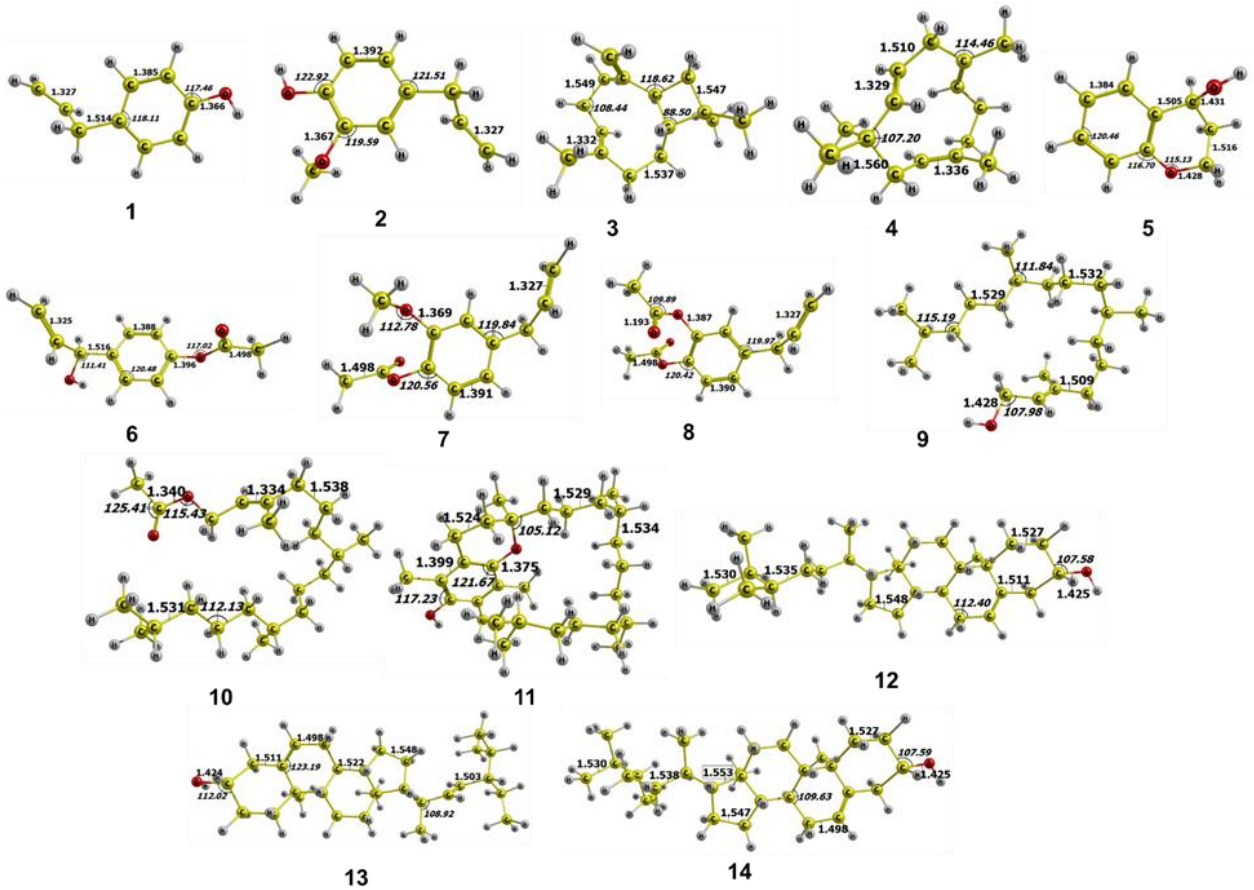

Fig. 2. Geometrically optimized structures of **1-14**

pISSN 1859-1388
eISSN 2615-9678

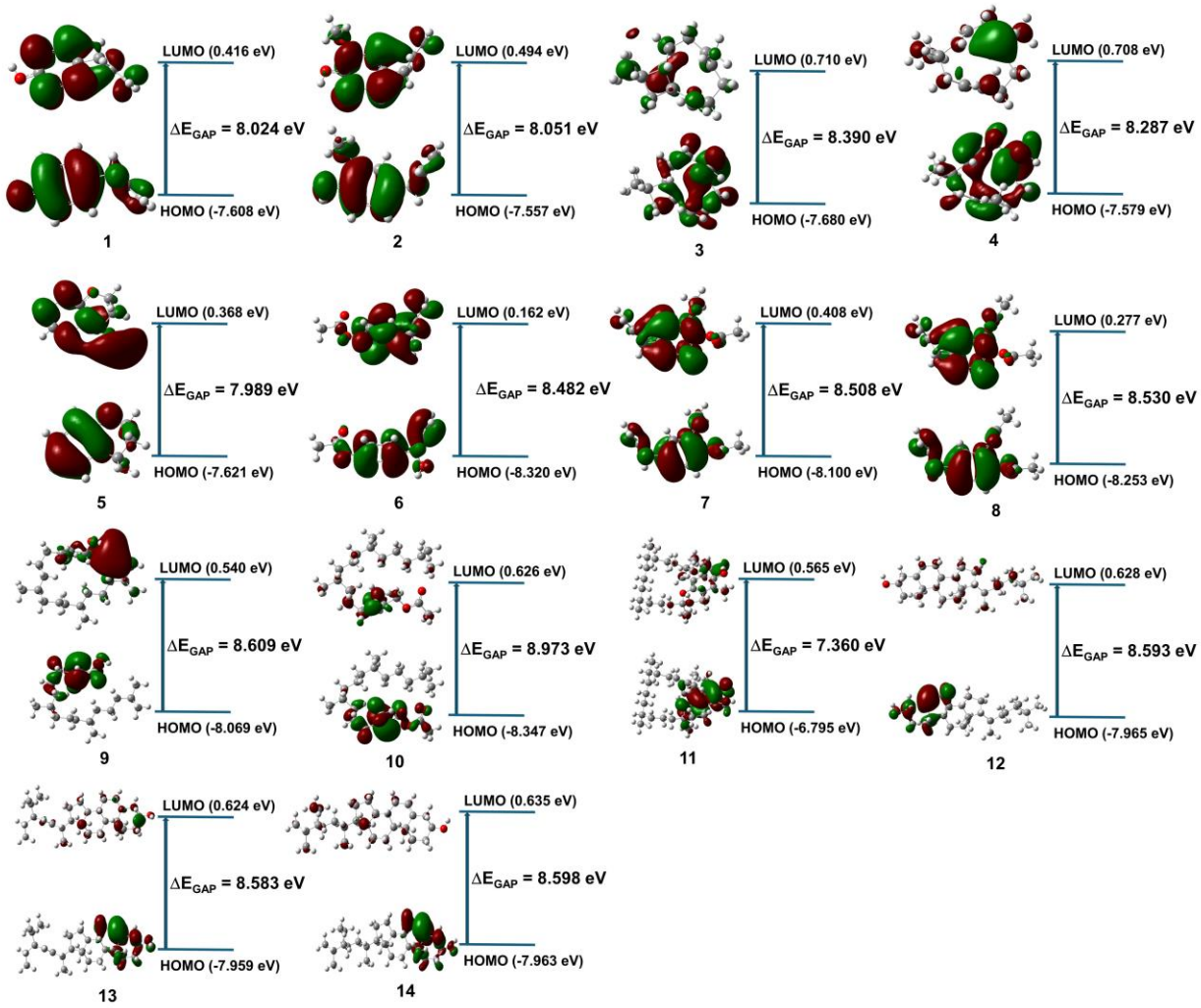

Fig. 3. Frontier molecular orbitals (HOMO and LUMO) of **1-14**

Table 2. Ground state electronic energy and dipole moment values of **1-14**

Notation	**Ground state electronic energy** (a.u.)	**Dipole moment** (Debye)
1	-424.24	1.55
2	-538.78	2.32
3	-586.07	0.39
4	-586.07	0.46
5	-499.50	2.61
6	-652.15	2.82
7	-691.45	2.89
8	-804.83	0.77
9	-861.55	2.25
10	-1014.24	2.19
11	-1285.88	1.02
12	-1171.31	1.76
13	-1209.40	2.20
14	-1210.63	1.80

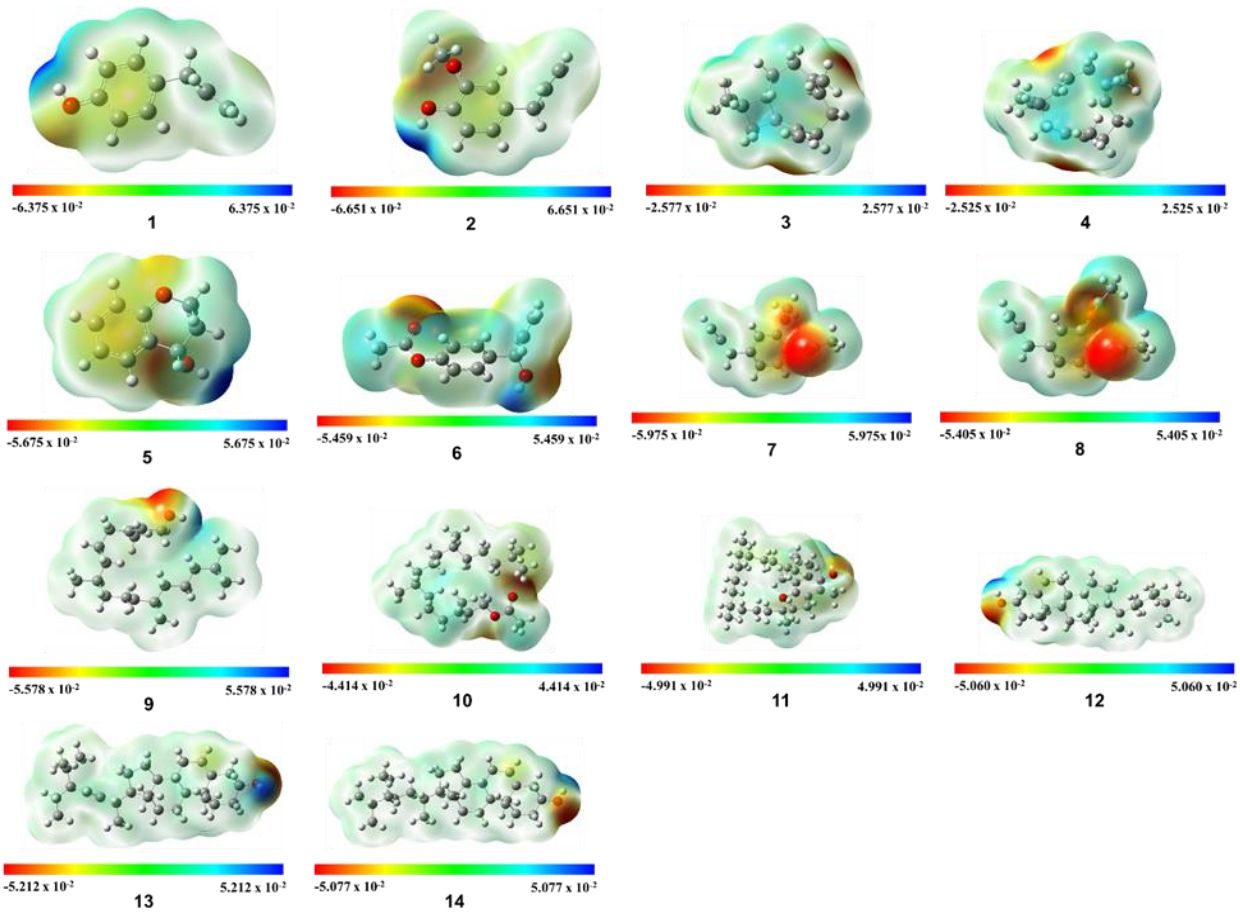

Fig. 4. Molecular electrostatic potential (MEP) of **1-14**

3.3 Docking-based inhibitability

The inhibitory potential of each candidate toward specific protein structures is assessed by the docking technique. The results from docking technique provide the inhibitory properties of each bioactive compound in the view of specific complex structures. This monitors the static interactions between the ligands (**1-14**) and their targeted protein 3DEA. In essence, the total docking score (DS) values (representing pseudo Gibbs free energy) are selected as the main indicator for inhibitory effectiveness.

Table 3 summarized the in-detail data regarding each ligand-3DEA complex. Given the theoretical interpretation, the most effective ligand-3DEA inhibitory structures are **14-3DEA** (-11.1 kcal.mol^{-1}) and **9-3DEA** (-11.0 kcal.mol^{-1}), which are comparable to the corresponding figure of **D-3DEA** (-11.4 kcal.mol^{-1}). They are followed by the order of inhibitory significance, i.e.: **6-3DEA** (-10.9 kcal.mol^{-1}) > **5-3DEA** (-10.8 kcal.mol^{-1}) > **13-3DEA** (-10,4 kcal.mol^{-1}) > **12-3DEA** (-10.2 kcal.mol^{-1}) > **11-3DEA** (-10.0 kcal.mol^{-1}). Particularly, the predominant component, i.e. 5, is also predicted to register considerably significant inhibitability (against *C. gloeosporioides* cutinase). Additionally, the Root-mean-square deviation (RMSD) measures the average distance between backbone atoms, typically below 2 Å, indicating the level of bio-conformational rigidity or the fitting between ligand and protein.

Figure 5 visualizes the corresponding in-site arrangements and interaction maps. The descriptive specifications encompass hydrogen-like bonding (illustrated by dashed arrows), van

pISSN 1859-1388
eISSN 2615-9678

der Waals interactions (depicted as blurry purple regions), and conformational fitness (represented by dashed contours). Examination of the 3D in-site arrangements reveals that the sites are notably open and spacious in comparison to the sizes of the inhibitors. This suggests that further modification or functionalization of the current ligand structures remains feasible. Analysis of the 2D maps indicates that the ligands are likely to exhibit good conformational fitness with the in-site features, as evidenced by the continuity of dashed contours.

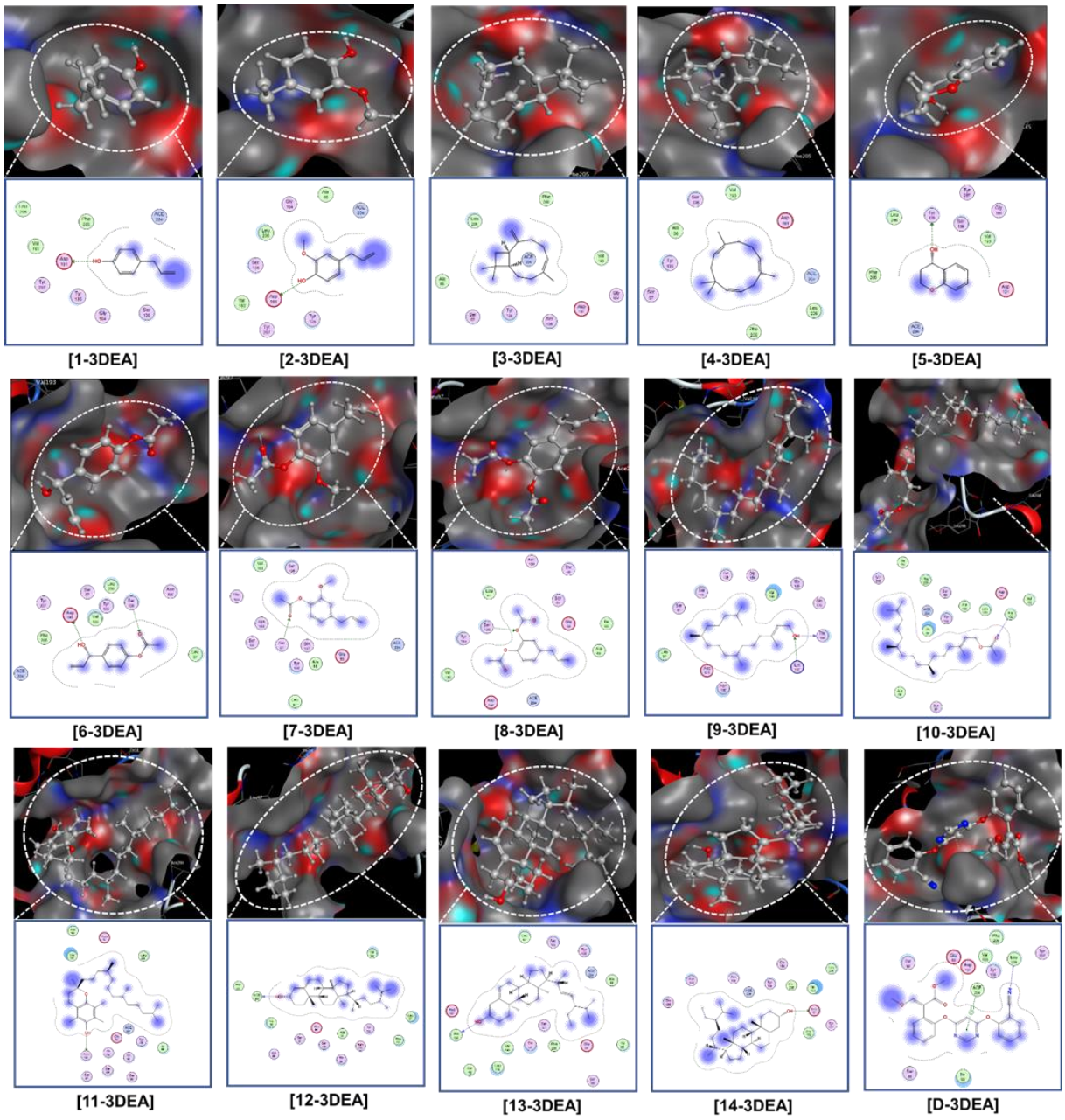

Fig. 5. Visual presentation and in-pose interaction map of ligand-3DEA inhibitory structures (ligand: **1-14** and **D**)

Table 3. Molecular docking simulation results for ligands (**1-14** and **D**)-3DEA inhibitory complexes

Ligand-protein complex			**Hydrogen bond**						**van der Waals interaction**
Name	**DS**	**RMSD**	**L**	**P**		**T**	**D**	**E**	
1-3DEA	-9.2	1.68	O	O	Asp 191	H-donor	2.84	-5.2	Leu206, Phe205, Ace204, Val193, Tyr207, Tyr135, Gly164, Ser136
2-3DEA	-9.6	1.81	O	O	Asp 191	H-donor	2.91	-4.6	Ala56, Ace204, Tyr135.Tyr207, Val193, Ser136, Leu206, Gly164
3-3DEA	-8.0	0.47	-	-	-	-	-	-	Leu206, Phe205, Val193, Gly164, Asp191, Ser136, Tyr135, Ser57, Ala56
4-3DEA	-8.1	1.67	-	-	-	-	-	-	Ser47, Tyr135, Ala56, Ser136, Val193, Asp191, Ace204, Leu206, Phe205
5-3DEA	-10.8	1.47	O	O	Tyr 135	H-donor	2.95	-0.9	Phe205, Leu206, Ser136, Tyr207, Val193, Gly164, Asp191, Ace204
6-3DEA	-10.9	0.93	O	O	Asp 191	H-donor	3.00	-1.3	Ace204, Phe205, Tyr207, Val193, Ser57.Tyr135.Leu206, Asn100, Leu97
			O	O	Ser 136	H-acceptor	2.96	-0.8	
7-3DEA	-9.5	1.19	O	O	Ser 57	H-acceptor	2.84	-2.9	Val193, Ser136, Ace204, Glu59, Ala56, Gln137, Tyr135, Leu97, Ser66, Asn100, Thr166
8-3DEA	-9.3	1.34	O	O	Ser 136	H-acceptor	2.86	-0.8	Asn100, Thr58, Ser57, Glu59, Ala56, Ile65, Ace204, Asp191, Val193, Tyr135, Leu97
9-3DEA	-11.0	1.66	O	O	Thr 166	H-donor	2.89	-1.6	Leu97.Ser57, Ser136, Tyr135, Gly164, Val193, Gly196, Gln170, Asn100, Asp191
			O	N	Lys 167	H-acceptor	3.47	-0.9	
10-3DEA	-9.7	1.34	O	N	Ala 192	H-acceptor	3.23	-0.8	Ala56, Ser57, Val193, Asp191, Leu206, Ala190, Tyr135, Ile65, Ace204, Ser66, Phe205, Ile70, Gln208
11-3DEA	-10.0	1.93	O	O	Asn 100	H-donor	2.95	-0.9	Ala192, Val193, Asp191, Leu206, Ace204, Glu59, Thr166, Ser136, Ser57, Tyr135, Thr58, Ser66, Ile65
12-3DEA	-10.2	1.81	O	O	Ace 204	H-donor	2.84	-1.1	Val193, Leu97, Phe101, Tyr135, Asn100, Ala56, Thr58, Ser136, Glu59, Ser57, Ser66, Ile65, Phe205
13-3DEA	-10.4	0.91	O	O	Ala 190	H-donor	2.96	-1.1	Leu97, Ser136, Tyr135, Ace204, Ala56, Ile65, Glu59, Ser66, Phe205, Ser57, Thr58, Val193, Leu206, Ala192, Asp191
14-3DEA	-11.1	1.26	O	O	Asp 191	H-donor	3,03	-2.2	Thr166, Asn100, Ser136, Ace204, Tyr135, Gly164, Phe205, Val193, Leu206, Tyr207, Ala192
			O	O	Asp 191	H-donor	3.10	-0.9	
D-3DEA	-11.4	1.85	N	N	Leu 206	H-acceptor	3.29	-2.9	Thr58, Glu59, Asp191, Val193, Tyr135, Phe205, Tyr207, Ile65, Ser66
			6-ring	C	Ace 204	π-H	3.11	-0.8	

DS: Docking score energy (kcal.mol^{-1}); **RMSD**: Root-mean-square deviation (Å);
L: Ligand; **P**: Protein; **T**: Type; **D**: Distance (Å); **E**: Energy (kcal.mol^{-1})

pISSN 1859-1388
eISSN 2615-9678

Table 4. Pharmacokinetic and pharmacological properties of compounds **1-8**

Property	1	2	3	4	5	6	7	8	Unit
Absorption									
Water solubility	-1.994	-2.004	-5.515	-5.191	-1.311	-2.153	-3.273	-3.332	(1)
Caco2 permeability	1.529	1.587	1.428	1.421	1.622	1.234	1.536	1.31	(2)
Intestinal absorption	92.983	93.514	94.827	94.682	94.143	94.351	97.801	97.549	(3)
Skin Permeability	-1.417	-2.299	-1.601	-1.739	-2.449	-2.575	-2.497	-2.642	(4)
P-glycoprotein substrate	No	No	No	Yes	No	No	No	No	(5)
P-glycoprotein I inhibitor	No	No	No	No	No	No	No	No	(5)
P-glycoprotein II inhibitor	No	No	No	No	No	No	No	No	(5)
Distribution									
VDss	0.383	0.458	0.645	0.505	0.071	0.034	0.015	-0.229	(6)
Fraction unbound	0.337	0.393	0.263	0.347	0.388	0.368	0.285	0.271	(6)
BBB permeability	0.328	0.471	0.74	0.663	-0.004	0.074	0.299	0.015	(7)
CNS permeability	-1.808	-2.012	-2.182	-2.555	-2.214	-2.263	-2.134	-2.359	(8)
Metabolism									
CYP2D6 substrate	No	No	No	No	No	No	No	No	(5)
CYP3A4 substrate	No	No	No	No	No	No	No	No	(5)
CYP1A2 inhibitor	Yes	Yes	No	No	No	Yes	Yes	Yes	(5)
CYP2C19 inhibitor	No	No	No	No	No	No	No	No	(5)
CYP2C9 inhibitor	No	No	Yes	No	No	No	No	No	(5)
CYP2D6 inhibitor	No	No	No	No	No	No	No	No	(5)
CYP3A4 inhibitor	No	No	No	No	No	No	Yes	No	(5)
Excretion									
Total Clearance	0.269	0.288	1.088	1.282	0.277	0.416	0.485	0.624	(9)
Renal OCT2 substrate	No	No	No	No	No	No	No	No	(5)
Toxicity									
AMES toxicity	No	No	No	No	No	No	Yes	No	(5)
Max. tolerated dose	1.014	0.773	0.429	0.551	0.806	1.045	1.355	1.477	(10)
hERG I inhibitor	No	No	No	No	No	No	No	No	(5)
hERG II inhibitor	No	No	No	No	No	No	No	No	(5)
Oral Rat Acute Toxicity	1.709	2.129	1.634	1.766	1.943	2.1	1.892	2.014	(11)
Oral Rat Chronic Toxicity	2.035	2.297	1.407	1.336	2.419	1.956	2.09	2.036	(12)
Hepatotoxicity	No	No	No	No	No	No	No	No	(5)
Skin Sensitization	Yes	Yes	Yes	Yes	Yes	No	Yes	No	(5)
T. Pyriformis toxicity	0.148	0.56	1.399	1.451	0.333	0.778	0.782	0.664	(13)
Minnow toxicity	1.38	1.515	0.506	0.716	1.871	1.241	1.307	1.044	(14)

(1) log $mol.L^{-1}$; (2) log Papp (10^{-6} $cm.s^{-1}$); (3) %; (4) log Kp; (5) Yes/No; (6) log $L.kg^{-1}$; (7) log BB; (8) log PS; (9) log $mL.min^{-1}.kg^{-1}$; (10) log $mg.kg^{-1}.day^{-1}$; (11) $mol.kg^{-1}$; (12) log $mg.kg^{-1}\_bw.day^{-1}$; (13) log $\mu g.L^{-1}$; (14) log mM

Table 5. Pharmacokinetic and pharmacological properties of compounds **9-14** and **D**

Property	9	10	11	12	13	14	D	Unit
Absorption								
Water solubility	-7.546	-7.689	-8.221	-7.194	-6.882	-6.957	-4.709	(1)
Caco2 permeability	1.52	1.179	1.245	1.284	1.28	1.267	1.554	(2)
Intestinal absorption	91.162	93.275	91.466	95.749	96.39	95.884	92.495	(3)
Skin Permeability	-2.569	-2.769	-2.716	-2.756	-2.702	-2.705	-2.737	(4)
P-glycoprotein substrate	No	No	Yes	No	No	No	No	(5)
P-glycoprotein I inhibitor	No	No	No	Yes	Yes	Yes	Yes	(5)
P-glycoprotein II inhibitor	Yes	Yes	Yes	Yes	Yes	Yes	Yes	(5)
Distribution								
VDss	0.478	0.365	0.901	0.351	0.102	0.12	-0.451	(6)
Fraction unbound	0	0	0	0	0	0	0	(6)
BBB permeability	0.811	0.772	0.857	0.804	0.814	0.824	-1.228	(7)
CNS permeability	-1.566	-1.607	-1.379	-1.43	-1.326	-1.379	-3.277	(8)
Metabolism								
CYP2D6 substrate	No	No	No	No	No	No	No	(5)
CYP3A4 substrate	Yes	Yes	Yes	Yes	Yes	Yes	Yes	(5)
CYP1A2 inhibitor	Yes	Yes	No	No	No	No	Yes	(5)
CYP2C19 inhibitor	No	No	No	No	No	No	No	(5)
CYP2C9 inhibitor	No	No	No	No	No	No	Yes	(5)
CYP2D6 inhibitor	No	No	No	No	No	No	No	(5)
CYP3A4 inhibitor	No	No	No	No	No	No	Yes	(5)
Excretion								
Total Clearance	1.686	1.684	0.812	0.572	0.618	0.628	0.777	(9)
Renal OCT2 substrate	No	No	No	No	No	No	No	(5)
Toxicity								
AMES toxicity	No	No	No	No	No	No	No	(5)
Max. tolerated dose	0.133	0.174	0.569	-0.193	-0.385	-0.341	0.759	(10)
hERG I inhibitor	No	No	No	No	No	No	No	(5)
hERG II inhibitor	Yes	No	Yes	Yes	Yes	Yes	No	(5)
Oral Rat Acute Toxicity	1.603	1.622	2.057	2.355	2.836	2.854	2.402	(11)
Oral Rat Chronic Toxicity	1.043	2.927	3.042	1.125	1.102	1.085	1.349	(12)
Hepatotoxicity	No	No	No	No	No	No	Yes	(5)
Skin Sensitization	Yes	Yes	No	No	No	No	No	(5)
T. Pyriformis toxicity	1.903	1.587	1.275	0.676	0.481	0.477	0.287	(13)
Minnow toxicity	-1.59	-1.916	-3.088	-2.071	-1.952	-2.079	-0.03	(14)

(1) log $mol.L^{-1}$; (2) log Papp (10^{-6} $cm.s^{-1}$); (3) %; (4) log Kp; (5) Yes/No; (6) log $L.kg^{-1}$; (7) log BB; (8) log PS; (9) log $mL.min^{-1}.kg^{-1}$; (10) log $mg.kg^{-1}.day^{-1}$; (11) $mol.kg^{-1}$; (12) log $mg.kg^{-1}\_bw.day^{-1}$; (13) log $\mu g.L^{-1}$; (14) log mM

pISSN 1859-1388
eISSN 2615-9678

3.4 ADMET-based pharmacological potentiality

The ADMET properties of the compounds are separated into Table 4 (**1-8**) and Table 5 (**9-14** and **D**), including chemical absorption, distribution, metabolism, excretion, and toxicity. These characteristics are not directly related to the candidates as potential fungicides, but are extensively regarded for potential effects to the body as the pesticide residue.

Regarding absorption, all candidates can be effectively absorbed through the intestinal tract by an absorbance > 90 % (considered poor if under 30 %) and low-to-none interaction with P-glycoprotein (no effects to the extrusion of the toxins and xenobiotics out of cells) is predicted. This means they are considered highly suitable for administration via oral intake. Regarding distribution, the total extract sees a plasma-tissue balance (-0.15 < log VDss < 0.45), partially crosses the blood-brain barrier (logBB > 0.3) and partially penetrates the central nervous system (-3 < log PS < -2). The properties implicate that the natural source appears to widely pose their effects throughout the body. Regarding metabolism, almost no significant interaction (either as inhibitors or substrates) to the cytochromes P450 family. This indicates that they are not oxidized by the liver and might have a longer span in the body. Regarding excretion, all the compounds are predicted not under the disposition (renal clearance) by Organic Cation Transporter 2. This, to certain extent, implies that the active agents can remain longer in the physiological circulation, thus retaining time-extended pharmacological effects. In terms of toxicity, they are considered significantly safe for use in humans: (i) except for **7**, no mutagenic potentials (AMES toxicity); (ii) low potential for fatal ventricular arrhythmia (hERG inhibition); (ii) no potential for hepatotoxicity; (iv) toxicity to bacterium *T. Pyriformis* (pIGC50 > -0.5 log $\mu g.L^{-1}$ yet no effects against fish Flathead Minnows (LC50 > -0.3). Although predicted for its AMES potent, Eugenol actate (**7**) has been long used for dental clinics without explicit warnings for adverse indications or long-term effects [23,35]; thus, the indirect applications as green pesticidal alternatives in this work further impose less concern regarding the residual traces remaining.

4 Conclusions

This study extends the as-evidenced promising fungicidal potentiality of *P. betle* L ethanol-extract compounds (**1-14**) against *C. gloeosporioides* based on computational models. Quantum-chemical dipole moment values especially indicate the favoured bio-medium compatibility of compounds **5-7**, **9-10**, and **13** (over 2 Debye). Docking-inhibitory DS values suggests the most promising inhibitors against *C. gloeosporioides* cutinase representative into the order: **14-3DEA** (-11.1 $kcal.mol^{-1}$) > **9-3DEA** (-11.0 $kcal.mol^{-1}$) > **6-3DEA** (-10.9 $kcal.mol^{-1}$) > **5-3DEA** (-10.8 $kcal.mol^{-1}$) > **13-3DEA** (-10,4 $kcal.mol^{-1}$) > **12-3DEA** (-10.2 $kcal.mol^{-1}$) > **11-3DEA** (-10.0 $kcal.mol^{-1}$). ADMET-regressive model considers the total extract with safety and suitability for pharmacological purposes. Altogether, the results consistently associate certain primary constituents of *P. betle* L ethanol-extract, i.e. **5** (4-Chromanol) and **6** (1′-Hydroxychavicol acetate) to the total antifungal activity (against *C. gloeosporioides*), thus conducive to the use as a cost-effective green pesticide in its raw extract.

Acknowledgement

This study is the result of Provincial Science and Technology Project [No. TTH.2021-KC.12] funded by Vietnam Governmental Budget under regulation of Thua Thien Hue province.

Nguyen Thi Ai Nhung acknowledges the partial support of Hue University under the Core Research Program [Grant Number: NCTB.DHH.2024.04]

Conflicts of interest

The authors declare that there is no conflict of interest regarding the publication of this article.

References

1. Budgin JB, Flaherty MJ. Alternative therapies in veterinary dermatology. Vet Clin Small Anim Pract. 2013;43(1):189-204.
2. Tresch M, Mevissen M, Ayrle H, Melzig M, Roosje P, Walkenhorst M. Medicinal plants as therapeutic options for topical treatment in canine dermatology? A systematic review. BMC Vet Res. 2019;15(1):1-19.
3. Man LQ, Ly NT, Lan TT, Huy NX. Cloning, expression, and purification of truncated s1 epitope and peptide CT24 fusion protein of porcine epidemic diarrhea virus in Escherichia coli. Plant Cell Biotechnol Mol Biol. 2019;112-8.
4. Marín A, Ferreres F, Tomás-Barberán FA, Gil MI. Characterization and quantitation of antioxidant constituents of sweet pepper (Capsicum annuum L.). J Agric Food Chem. 2004;52(12):3861-9.
5. Sahitya UL, Sri Deepthi R, Krishna M. Anthracnose, a prevalent disease in capsicum. Res J Pharm Biol Chem Sci. 2014;5(3):1583-604.
6. Isaac S. Fungal-plant interactions. Springer Science & Business Media; 1991.
7. Dean R, Van Kan JAL, Pretorius ZA, Hammond-Kosack KE, Di Pietro A, Spanu PD, et al. The Top 10 fungal pathogens in molecular plant pathology. Mol Plant Pathol. 2012;13(4):414-30.
8. Than PP, Jeewon R, Hyde KD, Pongsupasamit S, Mongkolporn O, Taylor PWJ. Characterization and pathogenicity of Colletotrichum species associated with anthracnose on chilli (Capsicum spp.) in Thailand. Plant Pathol. 2008;57(3):562-72.
9. Kim KD, Oh BJ, Yang J. Differential interactions of a Colletotrichum gloeosporioides isolate with green and red pepper fruits. Phytoparasitica. 1999;27(2):97-106.
10. Sharma PN, Kaur M, Sharma OP, Sharma P, Pathania A. Morphological, pathological and molecular variability in Colletotrichum capsici, the cause of fruit rot of chillies in the subtropical region of north-western India. J Phytopathol. 2005;153(4):232-7.
11. Lakshmesha KK, Lakshmidevi N, Mallikarjuna SA. Changes in pectinase and cellulase activity of Colletotrichum capsici mutants and their effect on anthracnose disease on capsicum fruit. Arch Phytopathol Plant Prot. 2005;38(4):267-79.
12. Byung SK. Country report of anthracnose research in Korea. In: First International Symposium on Chili Anthracnose. Seoul: Hoam Faculty House, Seoul National University; 2007. p. 24.
13. Don LD, Van TT, Phuong Vy TT, Kieu PT. Colletotrichum spp. attacking on chilli pepper growing in Vietnam. Country report. In: Abstracts of the First International Symposium on Chilli Anthracnose. Republic of Korea: National Horticultural Research Institute, Rural Development of Administration; 2007. p. 24.
14. Nyon MP, Rice DW, Berrisford JM, Hounslow AM, Moir AJG, Huang H, et al. Catalysis by Glomerella cingulata cutinase requires conformational cycling between the active and inactive states of its catalytic triad. J Mol Biol. 2009;385(1):226-35.
15. Rodrigues ET, Lopes I, Pardal MÂ. Occurrence, fate and effects of azoxystrobin in aquatic ecosystems: a review. Environ Int. 2013;53:18-28.
16. Staub T. Fungicide resistance: practical experience with antiresistance strategies and the role of integrated use. Annu Rev Phytopathol. 1991;29(1):421-42.
17. Voorrips RE, Finkers R, Sanjaya L, Groenwold R. QTL mapping of anthracnose (Colletotrichum spp.) resistance in a cross between Capsicum annuum and C. chinense. Theor Appl Genet. 2004;109:1275-82.
18. Shinjini M RD, Pramathadhip P KM. Anti-Oxidant and Anti-Inflammatory Activities of Different Varieties of Piper Leaf Extracts (Piper Betle L.). J Nutr Food Sci. 2015;05(05):415.
19. Voon Wendy WY, Ghali AN, Rukayadi Y, Meor Hussin AS. Application of betel leaves (Piper betle L.) extract for preservation of homemade chili bo. Int Food Res J. 2014;21(6):2399-403.
20. Ravindran PN, Pillai GS, Balachandran I, Divakaran M. Galangal. In: Handbook of herbs and spices. Elsevier; 2012. p. 303-18.

pISSN 1859-1388
eISSN 2615-9678

21. Madhumita M, Guha P, Nag A. Extraction of betel leaves (Piper betle L.) essential oil and its bio-actives identification: Process optimization, GC-MS analysis and anti-microbial activity. Ind Crops Prod. 2019;138:111578.

22. Ahmed S, Zaman S, Ahmed R, Uddin MN, Acedo Jr A, Bari ML. Effectiveness of non-chlorine sanitizers in improving the safety and quality of fresh betel leaf. LWT. 2017;78:77-81.

23. Singtongratana N, Vadhanasin S, Singkhonrat J. Hydroxychavicol and Eugenol Profiling of Betel Leaves from Piper betle L. Obtained by Liquid-Liquid Extraction and Supercritical Fluid Extraction. Agric Nat Resour. 2013;47(4):614-23.

24. Made N, Mara D, Nayaka W, Malida M, Sasadara V, Sanjaya DA, et al. Piper betle (L): Recent Review of Antibacterial and Antifungal Properties, Safety Profiles, and Commercial Applications. 2021;(L):1-21.

25. Hai NTT, Bui QT, Tran TAM, Nguyen DVQ, Phan TQ, Nguyen TL, et al. Inhibition of rice-blast fungus Magnaporthe oryzae by Piper betle extracts: in vitro evidence and in silico prediction. Vietnam J Catal Adsorpt. 2021;10(1S):74-80.

26. Frisch MJ, Trucks GW, Schlegel HB, Scuseria GE, Robb MA, Cheeseman JR, et al. Gaussian 09 Revision A.2. 2009.

27. Kassel LS. Density-functional exchange-energy approximation with correct asymptotic behavior. Phys Rev A. 1988;38(6):3098-100.

28. Schäfer A, Horn H, Ahlrichs R. Fully optimized contracted Gaussian basis sets for atoms Li to Kr. J Chem Phys. 1992;97(4):2571-7.

29. Chemical Computing Group ULC. Molecular Operating Environment (MOE) [Internet]. Version 2022.02. Montreal: Chemical Computing Group ULC; 2024.

30. Pires DEV, Blundell TL, Ascher DB. pkCSM: Predicting small-molecule pharmacokinetic and toxicity properties using graph-based signatures. J Med Chem. 2015;58(9):4066-72.

31. Rad AS, Ardjmand M, Esfahani MR, Khodashenas B. DFT calculations towards the geometry optimization, electronic structure, infrared spectroscopy and UV–vis analyses of Favipiravir adsorption on the first-row transition metals doped fullerenes; a new strategy for COVID-19 therapy. Spectrochim Acta Part A Mol Biomol Spectrosc. 2021;247:Article ID 119082.

32. Rosenberg B. Electrical Conductivity of Proteins. Nature. 1962;193:364-5.

33. Cordes M, Giese B. Electron transfer in peptides and proteins. Chem Soc Rev. 2009;38(4):892-901.

34. Kharkyanen VN, Petrov EG, Ukrainskii II. Donor-Acceptor model of electron transfer through proteins. J Theor Biol. 1978;73(1):29-50.

35. Farmakolojik Ö. Pharmacological and Toxicological Properties of Eugenol. Turk J Pharm Sci. 2017;14(2):201-6.